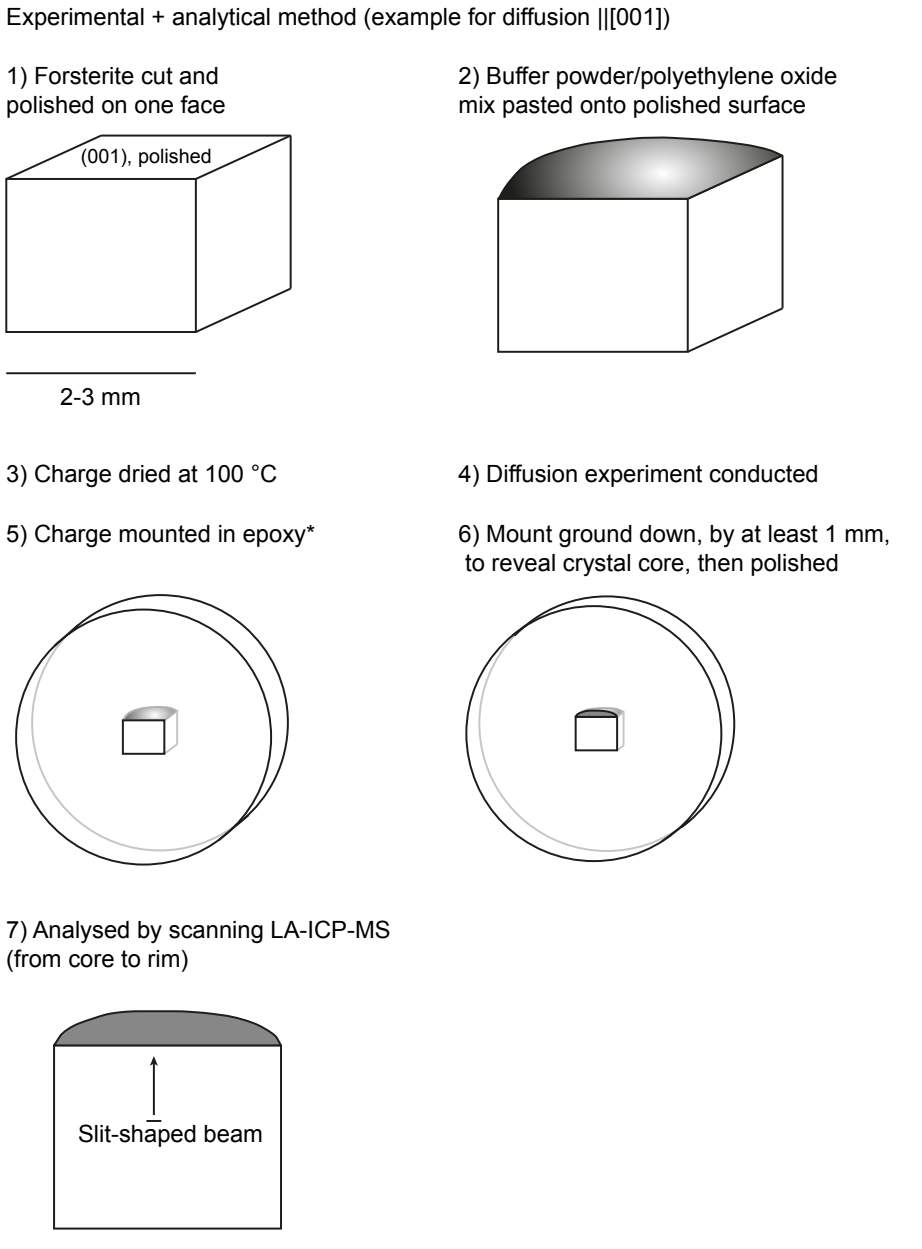

Supplemental Figure S1. Cartoon experimental and analytical procedure. (1) ~cubes of forsterite cut from a larger crystal, then polished on one face. Not shown: following cutting, forsterite was mounted in epoxy, ground and polished, then removed from the resin. (2) Buffer powder, sintered then re-ground, was mixed with polyethylene oxide glue, then pasted onto the crystal surface. The thickness was generally around 1 mm, which decreases considerably when the glue is dried, then devolatilised at run conditions. (3) Charge dried at 100 °C. (4) Diffusion experiment conducted in a tube or box furnace, with conditions described in the text. (5) Following the experiment, the charge was mounted in epoxy, and vacuum impregnated. This was often done with several other charges in the same mount. Sometimes the buffering powder was removed prior to mounting, other times it was not. (6) The mount was ground down on a diamond wheel by at least 1mm, to expose the crystal core. Then, the mount was diamond polished. (7) The sample was analysed by traversing a slit-shaped beam across the surface, from core to rim (i.e. from low ^{26}Mg to high ^{26}Mg). Note: no depth profiling was done in this study.

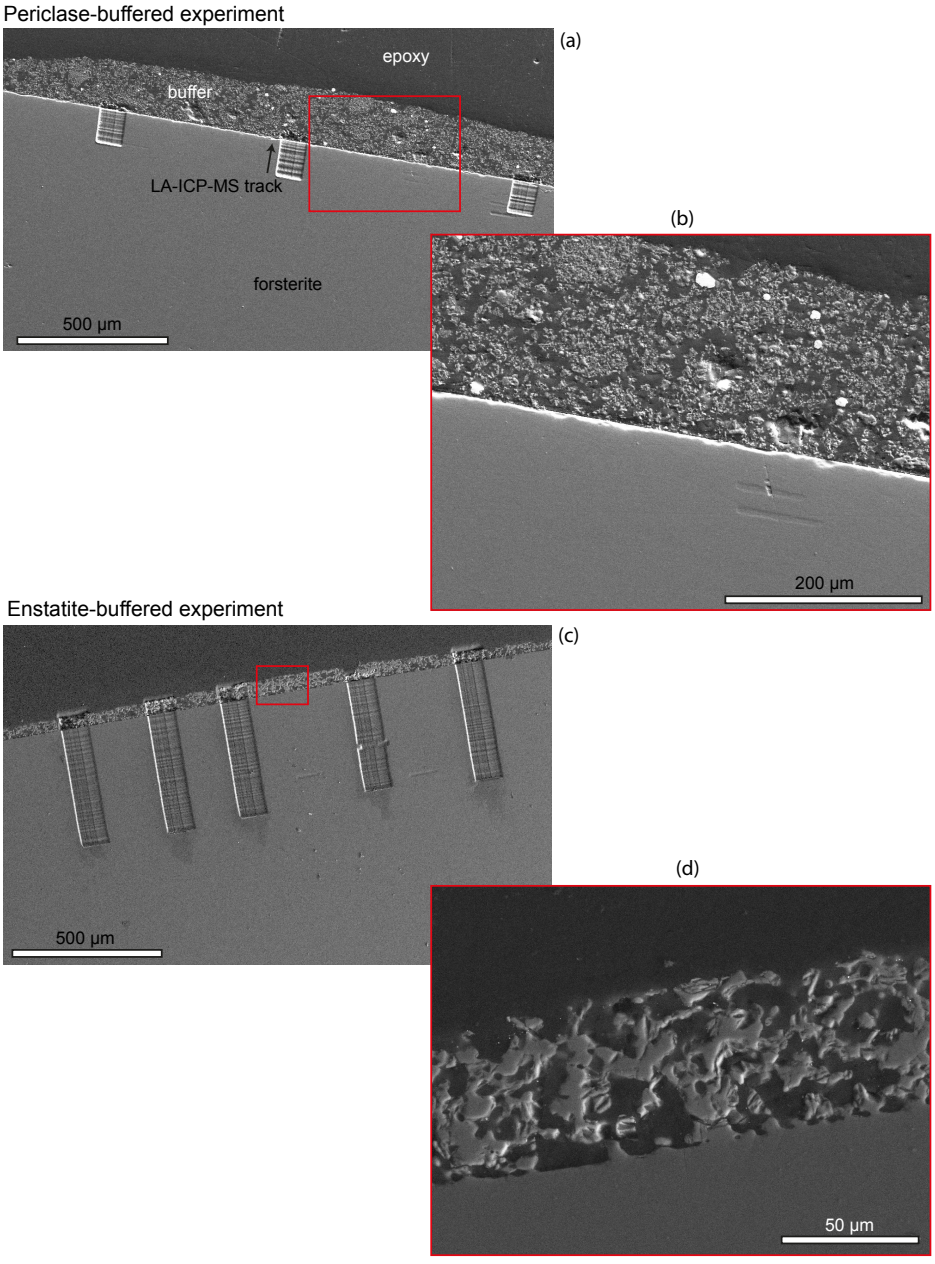

Supplemental Figure S2. Backscatter electron (BSE) images of the diffusion interface and buffering powder taken post-experiment using an Oxford Instruments CamScan scanning electron microscope (SEM) at the University of Lausanne. (**a**) fo-per buffered experiment, showing laser tracks. (**b**) enlargement of (**a**), showing surface roughness on the order of <10 µm. (**c**) and (**d**): as for (**a**) and (**b**), but for an enstatite buffered experiment. Note the longer laser tracks in (**c**) vs. (**a**), given that diffusivity is higher when buffered by fo-prEn compared to by fo-per.

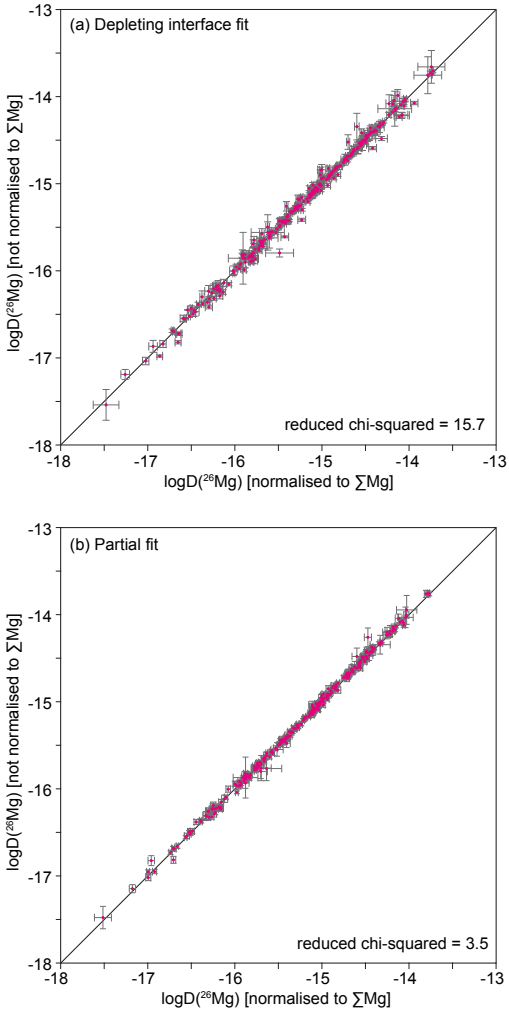

Supplemental Figure S3. Comparison of diffusion coefficients (^{26}Mg) determined following data reduction by the two methods. In both figures, the x axis is the diffusion coefficient determined after normalising to ΣMg, and the y axis is the diffusion coefficient determined when the data are not normalised to ΣMg. Reduced chi-squared are calculated from a 1:1 correlation. (**a**) is determined using the depleting interface solution (Eq. 5) and (**b**) using the fit to only part of the curve (Eq. 4).

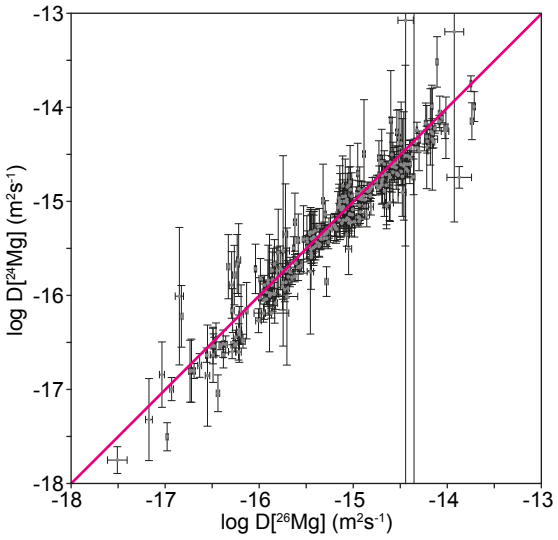

SUPPLEMENTAL FIGURE S4. Extracted diffusion coefficients for ^{26}Mg vs. ^{24}Mg, with uncertainties derived by combining the diffusion coefficients determined using the two fitting methods. Whilst the data cluster around the 1:1 line, the disagreementbetween diffusivities, and small uncertainties associated with ^{26}Mg, make the reduced chi squared too high to suggest a meaningful correlation.

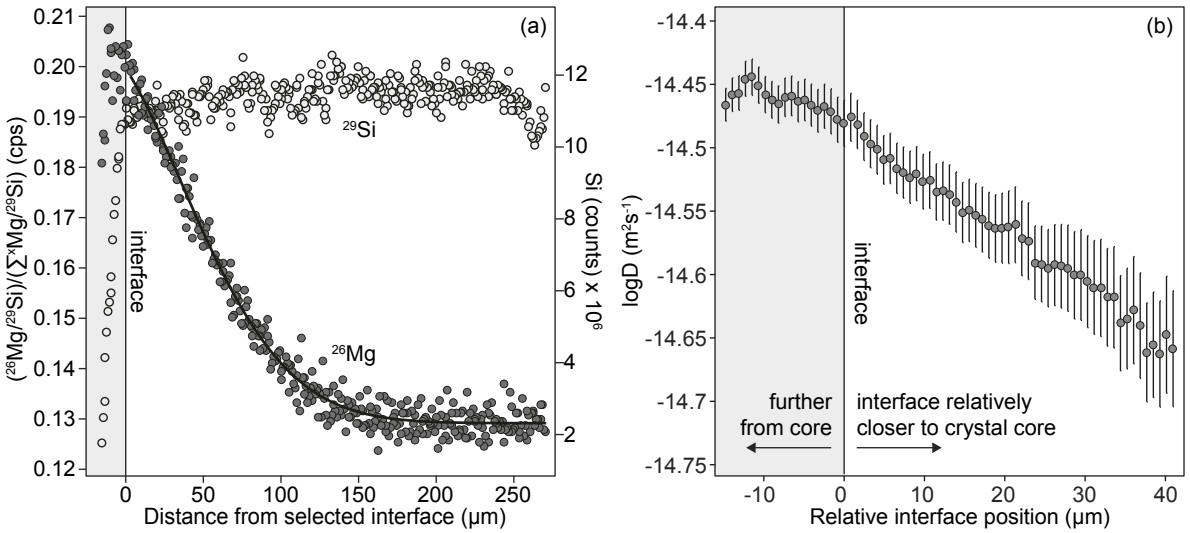

Supplemental Figure S5. The effect of chosen interface position on the outputted log*D* values. (**a**) Example ^{29}Si and ^{26}Mg profiles, and the chosen interface position associated with a drop in ^{29}Si counts. (**b**) the effect of moving the interface in either direction on diffusion coefficients, and their uncertainties.

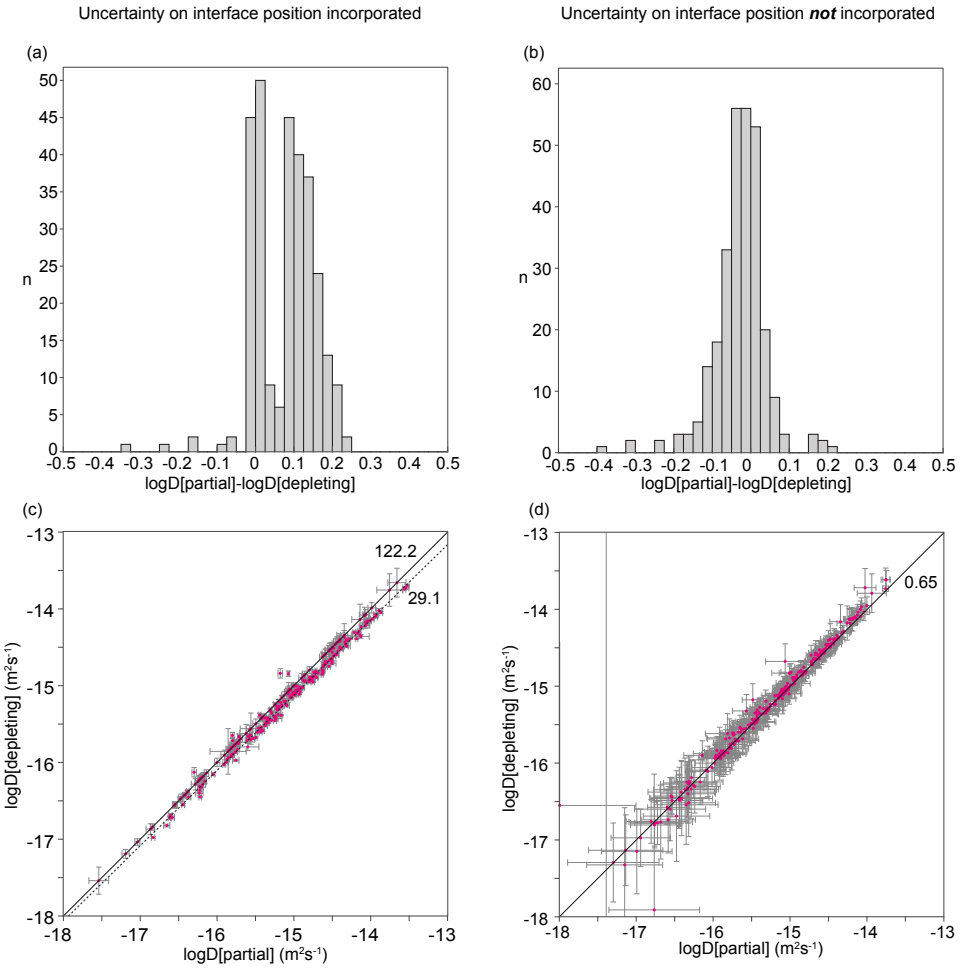

SUPPLEMENTAL FIGURE S6. Comparing the diffusivities extracted by fitting only the tail end of the diffusion profiles (partial fit) versus those determined using Equation 5, which assumes a linearly decreasing boundary condition. (**a**) histogram of the difference between *D* values determined using the two methods, showing a mean offset to around –0.1 (i.e. the partial fit method gives *D* values around 0.1 orders of magnitude lower than the depleting source method, when comparing medians). (**b**) all fits from the two methods, compared. Whilst the correlation appears strong, the reduced chi squared is extremely high, regardless of the fitting method used. This is because the errors from curve fitting are generally smaller than the discrepancy between *D* values from the two methods.

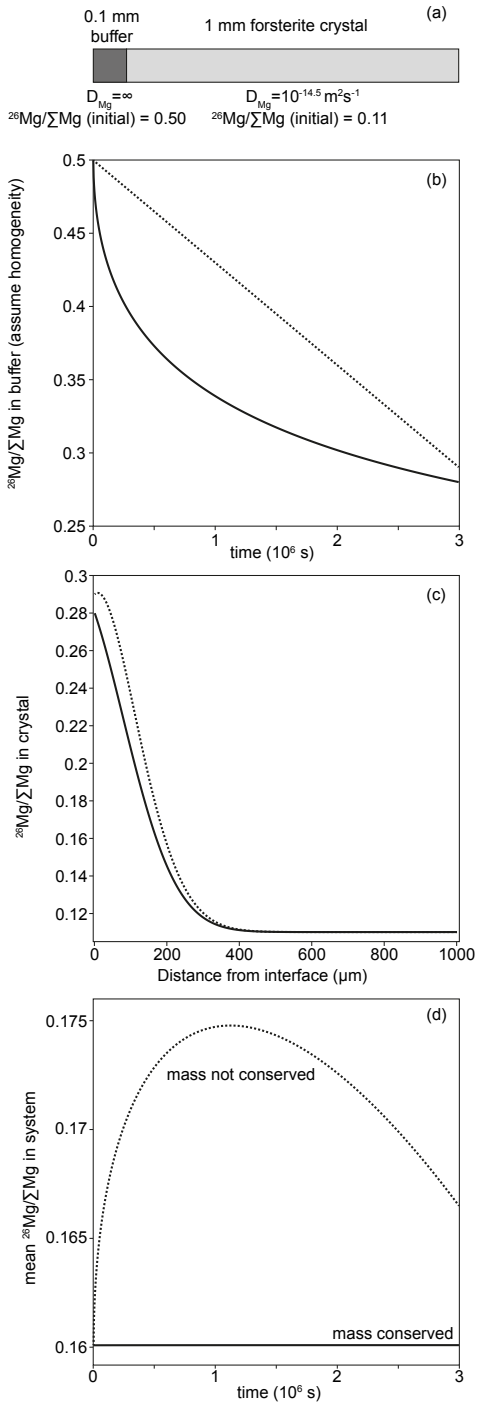

Supplemental Figure S7. Considering the validity of Equation 5 to such a system as studied in this work. (**a**) schematic of the (1D) model used. A 0.1 mm thick buffer powder, with infinitely fast diffusion (no Mg isotopic gradient within the buffer at any time) and enriched ^{26}Mg, is attached to a 1 mm long crystal, with defined *D* and the natural abundance of ^{26}Mg. For simplicity we assume length is proportional to mass. The model assumes no isotopic fractionation between buffer and crystal. All modelling is done using an explicit finite difference approximation of Fick's second law. (**b**) Comparison of the evolution of the boundary conditions over time. The dashed line shows the linear decrease assumed by Equation 5, whereas the solid line describes the evolution of the boundary when mass is conserved in the whole system, with a shape close to logarithmic. This was calculated by subtracting the total amount of ^{26}Mg in the crystal from the total ^{26}Mg in the whole system at every time step. (**c**) Diffusion profiles generated using the two boundary conditions. The linear decrease model predicts a slight inflexion in the near boundary, whereas the mass conservation model does not. (**d**) The total amount of ^{26}Mg in the system (given as mean isotopic ratio) over the duration of the model. The linear decrease boundary condition leads to ^{26}Mg increasing then decreasing, which is clearly not feasible in a closed system.

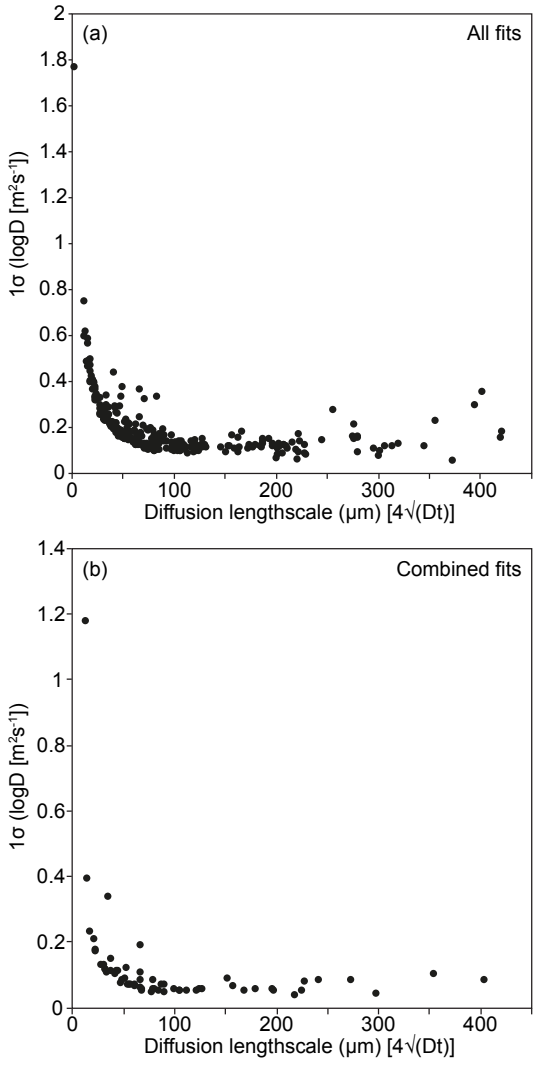

SUPPLEMENTAL FIGURE S8. The relationship between uncertainties and diffusion profile length. Uncertainties are calculated as described in the text, combining fits determined using the two solutions to the diffusion equation, and incorporating the x0 term that accounts for uncertainty on the interface position. The diffusion lengthscale is calculated using the $4\sqrt{(Dt)}$ approximation, which is an estimate of the distance over which the concentration decays by erf(2), i.e. by around 99.5%. (**a**) includes all fits, (**b**) is the data after multiple fits have been combined.